RSC Advances

ROYAL SOCIETY OF CHEMISTRY

www.rsc.org/advances

Effect of plasma nitriding on structure and biocompatibility of self organised TiO_2 nanotubes on Ti-6Al-7Nb.

L. Mohan [a, b], C. Anandan [a, *] N. Rajendran [b, *]

[a] *Surface Engineering Division, CSIR-National Aerospace Laboratories P.O.Box:1779, Old Airport Road, Bangalore, Karnataka, India*

[b] *Department of Chemistry, Anna University, Chennai, Tamilnadu, India*

Abstract

TiO_2 nanotubes formed by anodic oxidation of Ti-6Al-7Nb were nitrided in a nitrogen plasma. The samples were characterized by X-ray diffraction (XRD), X-ray photoelectron spectroscopy (XPS), Nano hardness tester (NHT) and Field emission scanning electron microscopy (FESEM). The corrosion behaviour of the substrate, plasma nitrided substrate, substrate with self organised TiO_2 nano tubes (TNT) and with plasma nitrided TiO_2 nano tubes (TNT+PN) was investigated through electrochemical impedance spectroscopy (EIS) and potentiodynamic polarization studies in simulated body fluid (Hanks' solution). The investigations show that the native oxide on the sample is replaced by self assembled nano array by anodisation process. XPS spectra of TNT plasma nitrided sample show the presence of oxy nitride and nitride on the surface. Nano hardness of the samples has increased after nitriding. FESEM images of samples immersed in Hanks' solution show that growth of calcium phosphate phases is more and the size of deposits are larger on TNT and nitrided TNT samples, as compared to that on the untreated substrate. XPS spectra of TNT and nitrided TNT samples immersed in Hanks' solution show higher amount of calcium, phosphorous and oxygen than on the substrate. Electrochemical studies show that nitriding decreases the corrosion resistance.

Keywords: anodic oxidation, nanotubes, nitriding, corrosion, EIS

*Corresponding authors E-mail addresses: canandan@nal.res.in (C. Anandan), nrajendran@annauniv.edu (N. Rajendran).

1. Introduction

Nowadays, nanostructured TiO_2 nano tubes are explored extensively for applications in different fields such as biomedical [1-3], photocatalysis [4, 5], sensing [6], and photovoltaic cell.[7] In case of bioimplants, titanium implants suffer from implant dislocation and premature loosening due to the fibrous encapsulation by tissue that isolates the implanted material from the surrounding bone and also because of its low chemical bonding ability with the bone. [8, 9] Implant surface properties will influence the extent of osseointegration. [10-13] Currently, researchers are focusing on surface modification of the implant at the nano-scale regime as bone cells are adapted to it.[14-16] Nanostructured materials are supposed to play a vital role in orthopaedic research due to the fact that structurally bone has a nanometre regime at the first level hierarchy.[17] Numerous studies have established that surfaces consisting of nanostructured TiO_2 on pure Ti show positive effect on cell behaviour such as substantial acceleration of apatite formation, improved proliferation, osteoblast adhesion and differentiation.[18-23] These results strongly suggested the use of nanostructured TiO_2 as a future implant material.

Due to high hardness and low coefficient of friction, titanium nitride (TiN) coatings allow improvement of the wear resistance of the substrate materials.[24, 25, 26] Thus, they are widely used in several industrial coating technologies. Further, it has been reported that, TiN coatings will enhance the corrosion resistance and biocompatibility of the Ti alloys.[27-29]

The purpose of the present study is to form titanium oxy nitride nanotubes on Ti-6Al-7Nb alloy by anodisation followed by plasma nitriding and characterize them for their nanoscale features, corrosion behaviour by electrochemical impedance spectroscopy (EIS) and potentiodynamic polarization studies in simulated body fluid (Hanks' solution).

2. Materials and methods

2.1 Preparation of the samples

Titanium alloy, Ti–6Al–7Nb (ASTM F1295 grade) was procured from TIMET, USA in the form of one inch diameter rod. Test samples of about ~3 mm thickness, cut from the rod were ground with different grades of silicon carbide papers and finally polished using 0.1μm diamond paste. These samples were ultrasonically cleaned using acetone and dried. A two electrode electrochemical anodisation cell, with platinum as cathode and Ti-6Al-7Nb substrate as anode, was used to fabricate the nanotube arrays. Anodisation was carried out at 20V with a DC power supply for 1 h. The anodic current density was monitored throughout the experiments. The electrode separation was kept constant at 2 cm. The electrolyte was made by mixing 50 ml of 0.08 (M) HF in 50 ml of 1(M) sulfuric acid. The electrolyte volume was held constant at 100 ml and continuously stirred using a magnetic stirrer. After anodization, plasma nitriding was performed in a vacuum chamber which is made up of stainless steel (304). The chamber was pumped to 2.4 x 10^{-6} millibar pressure by diffusion pump. Nitrogen flow was controlled by MKS make mass flow controllers. Nitriding was carried out at 1.4 x 10^{-4} millibar pressure. Plasma was generated using inductive coupling of 50W RF (13.56 MHz) power. The samples were kept in a tubular furnace kept inside the vacuum chamber and heated to 800ºC. The temperature of the sample was measured using a

thermocouple inside the vacuum chamber. The nitriding time was counted when the sample reached the desired temperature. After nitriding for the samples were cooled in vacuum to room temperature.

2.2. Immersion studies

Immersion studies were carried out on the substrate, nanotubes samples (TNT) and nanotubes nitrided samples (TNT + PN) by immersing them for 1 and 7 days at room temperature in freshly prepared acellular SBF (Simulated Body Fluid) Hanks' solution with ion concentrations that is nearly equal to that of human blood plasma (Na^+ =142.0, K^+ =5.0, Mg^{2+} = 1.5, Ca^{2+} = 2.5, HCO_3^- = 4.2, HPO_4^{2-} = 1.0, SO_4^{2-} = 0.50 and Cl^- = 147.96 mM). The chemical composition of the Hank's solution is as follows: 0.185 g $CaCl_2$, 0.4 g KCl, 0.06 g KH_2PO_4, 0.1 g $MgCl_2 \cdot 6H_2O$, 0.1g $MgSO_4 \cdot 7H_2O$, 8.0 g NaCl, 0.35 g $NaHCO_3$, 0.48 g Na_2HPO_4 and 1.00 g d-glucose in 1lit of milli-Q water. The pH of the solution was adjusted with 1M HCl to 7.2- 7.6.[30]

2.3. Electrochemical measurements

Electrochemical studies on the substrate and treated samples were conducted using CH 604D Electrochemical Workstation supplied by CH instruments, USA. The conventional three electrode glass cell was used to carry out the electrochemical studies. The tests were conducted in 200 ml of Hanks' solution which simulates the body fluid (SBF) at room temperature. The sample was kept as the working electrode (1 cm^2); Pt foil and saturated calomel electrode (SCE) were used as counter and reference electrodes, respectively. The reference electrode was kept very close to the surface of

the working electrode. The sample was immersed in Hanks' solution for an hour in order to establish the open circuit potential (E_{OCP}) or the steady state potential.

EIS measurement was carried out in the frequency range of 10 mHz to 100 kHz. The applied alternating sinusoidal potential was 10mV on the E_{OCP}. After each experiment, the impedance data were displayed as Bode plots. The Bode plot is a plot of log $|Z|$ vs. log f and log f vs. - phase angle (θ), where $|Z|$ is the absolute impedance and f is the frequency. The acquired data were curve fitted and analyzed using ZSimpwin program (Princeton Applied Research, USA) to get suitable equivalent circuit parameters. The quality of the fit was checked by the χ^2 value. After EIS measurements, potentiodynamic polarization studies were carried out in a potential range below 200 mV and above the OCP value with a scan rate of 1mV/s. The Tafel plot was obtained after the electrochemical measurements have been represented in the form of potential vs. log (i) plot. The corrosion potential (E_{corr}) and corrosion current (I_{corr}) were deduced from the Tafel plot.[31, 32]

2.4. Characterization techniques

The presence of various phases in the anodized samples was identified by X-Ray diffraction (XRD) using BRUKER D8 Advance, X-ray diffractometer. Monochromatic Cu Kα radiation (λ=0.1548 nm) was used and the samples were scanned from 20˚ to 80˚ at a scanning rate of 0.02°/min. Water Contact Angle (CA) of the samples was measured using Surface Electro Optics Phoenix contact angle meter (South Korea) by sessile drop method. Water droplets of about 8•0 µL were carefully dropped onto the samples through a syringe, and the CAs were obtained by measuring at different positions on each sample and the average value is reported. Nanohardness was measured

using a Nanohardness Tester (CSM instruments) with a Berkovich Diamond indenter at 0.5 mN load. The surface morphology of the samples was examined by Carl Zeiss Supra 40 VP FESEM. The 3D and 2D profiles of FESEM images were obtained by using the scanning probe image processor WSxM 5.0 develop 7.0 software.[33, 34] The composition of the TNT and TNT+PN samples immersed in SBF was analyzed by X-ray Photoelectron Spectroscopy (XPS). XPS spectra were obtained in a SPECS Surface Nano Analysis XPS system with 150W non-monochromatic Al Kα radiation with 1486.6eV energy. Core level spectra of Ti2p, N1s, O1s, Ca2p and P2p were obtained at a pass energy of 25eV. N1s and O1s core level spectra were fitted with Gaussian-Lorentzian peaks after subtracting Shirley background to find the component peaks using Casa-XPS software.

3. Results and discussion

Fig. 1 (a) shows the FESEM image of an anodic TiO_2 nano tube array (TNT) obtained after anodisation of Ti-6Al-7Nb for 1h at 20 V. **Fig. 1 (b)** shows the FESEM image of TNT plasma nitrided at 800°C (TNT +PN). **Figs. 1 (c and d)** show the 3D image of the TNT and TNT+PN obtained from FESEM image for the same respectively. In these images, the high degree of ordering of the tubes can be clearly seen. Similarly, **Figs. 1 (e and f)** show the 2D profile of the TNT and TNT+PN obtained from FESEM image for the same, respectively. FESEM images of the TNT and TNT+PN show that the arrays have very regular and vertically aligned tube structure. As indicated in **Figs. 1 (e and f)** in samples TNT and TNT+PN, the nano tubes have diameters of approximately ~100 and 80 nm and an average inter-tube distance of approximately ~30 and 35 nm respectively. The height of the nanotubes is approximately ~250 nm. Thus, there is no much change in tubular dimensions after nitriding.

In order to investigate the wettability of the samples, water contact angle was measured and the collected results are shown as insets in **Figs. 1 (a and b)**. In the insets, we compare the optical images of a water droplet on the as-prepared TNT and TNT +PN. The water contact angle is ~67.3˚ ±2.4 on Ti-6Al-4V substrate. On as-prepared TNT wetting by water was observed but after nitriding the TNT at 800˚C the water contact angle is 122˚±2. Thus, the sample becomes hydrophobic after nitriding. **Fig.2** shows the FESEM images of Ti-6Al-7Nb substrate and substrate after nitriding.

In **Fig. 3** XRD patterns (a) to (d) correspond to Ti-6Al-7Nb substrate, plasma nitrided substrate, as-formed TNT, and plasma nitrided nanotubes (TNT+PN) respectively. The location of different peaks pertaining to Ti, Ti-O-N, TiN and Ti_2N are shown in the figure. The substrate pattern **(a)** shows three dominant peaks due to Ti. In diffractogram **(b)**, for the nitrided sample, the intensity of the substrate diffraction peak at 38^o has nearly disappeared and appearance of peaks of the nitrides, TiN and Ti_2N can be seen after nitriding. In pattern (**d**), after nitriding of the TNTs, Ti-O-N, TiN and Ti_2N peaks can be observed. Also, the intensity of the Ti_2N phase is higher than that of TiN. This shows that predominantly Ti_2N is formed.

Nanohardness measurements were carried out on substrate, plasma nitrided substrate, TNT and TNT+PN samples at 0.5 mN load. Five indentations were taken at different locations to check the uniformity of the coating hardness. **Fig. 4** shows indentation curves taken on the sample and shows the uniformity of the coating hardness. **Figs. 5 (a and b)** show the FESEM images of samples after NHT on TNT and TNT+PN samples respectively. **Figs. 5 (c and d)** show the 3D image of the TiO_2 nano tube array generated from FESEM image for the same. Similarly, **Figs. 5 (e and f)** show the 2D profile of the nano indentation on TiO_2 nano tube array obtained from FESEM images after NHT. The hardness of the Ti-6Al-7Nb substrate is 9.2GPa, after plasma nitriding the hardness has increased to 15.5GPa. Similarly, the maximum displacement of the substrate and plasma nitrided

samples was 61 and 34nm respectively. This shows that nitriding will increase the surface hardness. Similarly, the hardness of the TNT and TNT+PN was 1.4 and 2.2 GPa, respectively. The maximum displacement of the TNT and TNT+PN was 144 and 95 nm respectively. The increase in the hardness and decrease in displacement suggest the nitriding of nanotubes which increases the hardness of the TNT. The sharp change of slope in the loading curves imply that after certain loading the tubular structure yields before resisting further deformation by increasing load. The unloading curves of the nanotubes show that there is no elastic recovery. This may be due to the fact that the nanotubes collapse after loading, which can be seen from the FESEM images in **Fig.5.** Even though a low load of 0.5mN has been used, the tubular structure collapses as the actual contact area is much lower due to the tubular structure. The hardness values are lower as compared to bulk oxide and nitride values for the same reason. The nano indentation studies show that the mechanical properties of the TNT+PN are better to that of TNT.

Fig. 6 shows the Ti2p, N1s and O1s core level XPS spectra from (a) TNT and nitrided (b) TNT samples, respectively. The at% of titanium, oxygen and nitrogen are given in **Table 1** for the same. In Ti2p spectrum **(a)** in **Fig. 6**, the surface is completely covered with TiO_2 has no trace of Ti metallic peak. This shows that the surface is completely covered by oxide after the anodization process. After nitriding, the Ti2p spectrum (**b**) in **Fig. 6** is broad. Various peaks representing titanium nitride (455.5eV), titanium oxide 458.9eV and intermediate peak around 456.8eV due to oxynitrides (TiO_xN_y) [35, 36] can be identified in the spectra. Also, the spectra have no trace of Ti metallic peak. This is because nitriding the titanium oxide nanotubes replaces the oxide by nitrides and oxynitrides.[37] In the N1s spectra, the high-intensity peak at ~396.86 eV corresponds to N in TiN and the low-intensity peak at a higher binding energy may be attributed to titanium oxynitride (TiNxOy).[38] The N1s core level spectra are fitted with these two components and the percentage of

each component is shown in **Table 1**. As can be seen in the table**,** the fraction of nitrogen is in oxynitride form. This oxynitride may have formed on nitriding of titanium oxide nanotubes. In Oxygen 1s core level spectra from TNT sample oxygen is bonded mostly as in metal oxide and hydroxide forms can be seen. Nitrided TNT samples contain three peaks can be identified in **Fig.6.** The main peak centered at 529.8 eV corresponds to O bonded to Ti. The other two peaks centered at 531.3 and 532.1 eV peaks correspond to oxygen bonded as in TiNxOy and as in hydroxyl groups .[39-41]

Figs. 7 (a), (b) and (c) show the FESEM images of the substrate, TNT and TNT+PN samples surfaces after 7 days immersion in Hanks' solution respectively. Insets in all the figures show the images at a higher magnification. In these images, formation of calcium phosphate phases (CP) appears as white deposit. The formation of the CP phases interact with water or body fluids to form hydroxyapatite [Ca_{10} $(PO_4)_6$ $(OH)_2$], HAp the principal component of bone material.[42] As can be seen in the images, the growth is more on the TNT and TNT+PN samples and the sizes of the deposits are also large. Insets in the figures at a higher magnification show that deposit have grown to larger size on the TNT and TNT+PN surface as compared to that on the substrate surface. The above observations point out that in addition to TNT, a TNT + PN sample also has higher potential for inducing growth of CP phases on the surface. This is further substantiated by the results of XPS to be discussed below.

Fig.8 compares the survey spectra from the substrate, TNT and TNT nitrided samples after 1 day immersion in Hanks' solution. XPS core level spectra of Ca2p, P2p and O1s from substrate, TNT and TNT+PN samples after 1 day immersion in Hanks' solution are shown in **Fig.9**. The binding energy of Ca 2p3/2 core level in **Fig. 9** is at 347.2eV and that of P2p3/2 is at 133.3eV.[43] These binding energies correspond to Ca in oxide form and P in phosphate form, both probably bonded as

apatite. Intensities of Ca2p and P2p XPS spectra are in the order: TNT > TNT+PN > substrate. **Table 2** gives the at% of various Ti2p, Ca2p, P2p and O1s in each case. These results show that Ca and P is more on the TNT and TNT nitrided samples. This implies that nitriding of TNT also facilitates growth of calcium phosphate phases on nano tube surface.

Potentiodynamic polarization curves of the substrate, nitrided substrate, TNT and TNT+PN samples in Hanks' solution are shown in **Fig. 10**. The corrosion current (I_{corr}) was obtained by extrapolation of the cathodic and anodic branches of the polarization curves to the corrosion potential. **Table 3** shows the corrosion current density and corrosion potential for the substrate, nitrided substrate, TNT and TNT+PN samples. The values of corrosion current density in **Table 3** show that nitriding has resulted in deterioration of corrosion resistance of the substrate. The corrosion current density of the TNT sample ($0.0158\mu A/cm^2$) shows that anodisation has not affected the corrosion resistance of the substrate. However, one point has to noted here. As compared to substrate, the surface area of TNT sample is much higher owing to the nano tube morphology. The increased corrosion current could be due to the increased area owing to this nanostructure of the system. Therefore, the actual corrosion resistance could very high. As in the case of substrate, nitriding has resulted in loss of corrosion resistance of the TNT sample. The E_{corr} value shifted to much nobler values for nitrided substrate and TNT samples (-0.188 and-0.236 V), compared to that of substrate value of −0.303 V indicating the passive nature of the nitrided substrate and TNT samples in Hanks' solution. There was no significant change in E_{corr} after nitriding TNT.

The results of electrochemical impedance tests in Hanks' solution for substrate, nitrided substrate, TNT and TNT+PN samples are presented in the form of Nyquist and Bode plots in **Figs. 11 (a, b, c and c)**. The Nyquist plots in **Fig. 11(a)** are semicircular with the substrate having a larger diameter in lower and higher frequencies **(Fig. 11 (a)** inset**).** The limiting impedance at the high frequency end

corresponds to solution resistance, R_e. In **Fig. 11 (b)**, for substrate and nitrided substrate, the phase angle changes rapidly from −0◦ to −20◦ in the high frequency range (10 to 100 kHz). In the low frequency range from 0.01 to 100 Hz, the phase angle remains nearly constant for substrate and nitrided substrate −82.5 and -79° respectively, which is less than the value for an ideal capacitor (−90°). In the same frequency range, a linear relationship between log |z| and log f is observed with a slope close to one. In the case of TNT**,** there is an inflexion point in the phase angle in the frequency range of 1 to 100 Hz. In the case of TNT+PN**,** there is a steady decrease of the phase angle in this frequency range. **Fig. 12 (a)** shows the equivalent circuit model used for fitting the EIS data of the substrate and nitrided substrate and **Fig. 12 (b)** shows the equivalent circuit model used for fitting the EIS data of the TNT and TNT+PN samples. The equivalent electrochemical circuit is composed of resistances and constant phase elements (CPE). The resistive components Re, R1 and R2 are related to the solution resistance, resistance of the outer porous layer and inner layer resistance, respectively. The Q symbol signifies the possibility of a non-ideal capacitance, known as constant phase element (CPE), and its impedance is defined as $ZCPE = [Q (j\omega^n)]^{-1}$ with 'n' less than 1; for an ideal capacitance n = 1. In this, Q1 represents the capacitance of the outer layer, Q2 the capacitance of the inner layer. Similar equivalent circuits have also been proposed for titanium alloys in Hanks' solutions by previous researchers.[44, 45]

In the case of TNT and TNT+PN samples, the equivalent circuit has three time constants and EC is given in **Fig. 12 (b)**. The outer porous oxide layer of the substrate is replaced by the inter-tube space. The inner barrier layer corresponds to the bottom of the nano tubes. The values of the electrical parameters obtained by fitting the impedance data of the substrate and anodized samples are given in **Table 3**. For the substrate and nitrided substrate, the high corrosion resistance R2 is associated with

inner layer on the substrate and nitrided substrate, which is 5.8× 10^6 and 5.4× 10^6 Ωcm^2 respectively, in the present case. The Q2 component is associated to the capacitance of this inner barrier layer. The resistance of outer porous layer is 21.5 Ωcm^2. The value "n" for the constant phase element representing the outer layer is 0.98 and 0.96 and that representing the inner layer is 0.92 and 0.88, respectively. In the case of TNT and TNT+PN samples the well formed nano tube structure acts an additional element in series with the substrate. The fitting parameters for TNT sample in **Table 4** shows that the resistance R1 of the outer layer is about 27.5Ωcm^2 and that of R2 is about 5.6x10^4 Ωcm^2. The high corrosion resistance R3 is associated with inner barrier layer of the nano tubes. The non ideal value for the constant phase element representing the Q1 and Q2 is 0.91 and 0.92 respectively and that representing the inner layer (R3) is 0.92.

In the case of TNT+PN samples (**Table 4**), the resistance R1 of the outer layer is 34.5Ωcm2 and that of R2 is 58Ωcm^2. There is deviation from near ideal capacitor behaviour in low frequency range (0.1 to 0.01 Hz) high, as the phase angle is ∼−75◦. However, resistance of the inner barrier layer R3, close to the substrate surface at the bottom of nanotubes, is high (5.2x10^4 Ωcm^2). The decreased corrosion resistance of nitrided and nitrided TNT samples show that the TiO_2 layer provides better corrosion resistance than nitrided surface.[46] However, nitriding of titanium alloys improve their tribological properties. Nitriding also helps in formation of calcium phosphate phases which leads to hydroxyapatite, the principle component of bone material.[39] It is well known that nano surface improves the adhesion of osteoblast and fibroblast cells to titanium alloys and also improve their bone forming ability.[18-23, 47] Above results show that nitriding results in nitrided TiO_2 nanotubes with better mechanical properties and biocompatibility. Therefore, nitriding nanotubes can be a promising method for surface modification of titanium for improving its biocompatibility.

Conclusions

Self-organized titanium oxide nanotube arrays with pore diameters ~100 nm have been formed on titanium alloy Ti-6Al-7Nb by anodic oxidation were nitrided in a nitrogen plasma. The XRD pattern of nitrided TNT sample show presence of Ti-O-N, TiN and Ti_2N peaks. Nanohardness measurements show an increase in hardness of TNTs due to nitriding. Potentiodynamic polarization and electrochemical impedance studies of TNT sample in Hanks' solution show that the corrosion resistance is comparable with that of substrate while corrosion resistance of nitrided substrate and TNT+PN samples is poorer than the substrate. Formation of calcium phosphate phases on TNT and TNT+PN samples is higher compared to that of substrate after 1 and 7 days immersion in Hanks' solution. Hence, nitriding of nano tubes helps in increasing the hardness of the TiO_2 nanotubes that enhances formation of CP phases.

Acknowledgments

The work was carried out under the CSIR network project on ESC-01-03. The authors would like to thank the Director, National Aerospace Laboratories, Bangalore for his support and permission to publish the work. The authors would like to thank Mr. Siju, Mr. Srinivas and Mr. Praveen, SED, NAL for FESEM, XRD and NHT studies.

References

1. Rodriguez R, Kim K, Ong JL, *J. Biomed. Mater. Res. A,* 2003, **65**,352.
2. Zinger O, Chauvy PF, Landolt D. *J. Electrochem. Soc.* 2003, **150**, B495.
3. Cai Q, Yang L, Yu Y, *Thin Solid Films,* 2006, **515**, 1802.
4. Roy P, Berger S, Schmuki P, *Angew Chem. Int. Ed.* 2011, **50**, 2904.
5. Jang HD, Kim SK, Kim SJ, *J. Nanopart. Res.* 2001, **3**, 141.
6. Varghese OK, Mor GK, Grimes CA, Paulose M, Mukherjee NA. *J. Nanosci. Nanotechnol.* 2004, **4**, 733.
7. Li D, Xia YN, *Nano. Lett.* 2003, **3**, 555.
8. Hong MH, Lee DH, Kim KM., Lee YK, *Surf. Interf. Anal.* 2010, **42 (6–7),** 492.
9. Bajgai MP, Parajuli DC, Park SJ, Chu KH, Kang HS, Kim HY, *J. Mater. Sci. Mater. Med.* 2010, **21 (2),** 685.
10. Lim J, Yu B, Woo K, Lee Y, *Appl. Surf. Sci.* 2008, **255 (5),** 2456.
11. Mohan L, Durgalakshmi D, Geetha M, Sankaranarayanan TSN, Asokamani R, *Ceram. Inter.* 2012, **38(4),** 3435.
12. Anandan C, Mohan L, Dilli Babu P, *Appl. Surf. Sci.* 2014, **296**, 86.
13. Zhang EW, Wang YB, Shuai KG, Gao F, Bai YJ, Cheng Y, Xiong XL, Zheng YF, Wei SC, *Biomed. Mater.* 2011, **6**, 025001.
14. Yu WQ, Qiu J, Zhang FQ, *Colloids Surf. B Biointerf.* 2011, **84 (2),** 400.
15. Indira K, Mudali UK, Rajendran N, *Ceram. Intern.* 2013, **39**, 959.
16. Indira K, Ningshen S, Mudali UK, Rajendran N, *Mater. Charact.* 2012, **71**, 58.
17. Minagar S, Berndt CC, Wang J, Ivanova E, Wen C, *Acta Biomater.* 2012, **8**, 2875.
18. Regonini D, Bowen CR, Jaroenworaluck A, Stevens R, *Mater. Sci. Engn. R,* 2013, **74**, 377.

19. Regonini D, Bowen CR, Stevens R, Allsopp D, Jaroenworaluck A, *Phys. Status. Solidi. A,* 2007, **204**, 1814.

20. Brammer KS, Choi C, Frandsen CJ, Oh S, Johnston G, Jin S, *Acta Biomater.* 2011, **7 (6),** 2697.

21. Huang Z, Daniels RH, Enzerink RJ, Hardev V, Sahi V, Goodman SB, *Tissue Eng. Part A,* 2008, **14 (11),** 1853.

22. Das K, Bose S, Bandyopadhyay A, *J. Biomed. Mater Res. A,* 2009, **90 (1)**, 225.

23. Dong W, Zhang T, Epstein J, Cooney L, Wang H, Li Y, Jiang YB, Cogbill A, Varadan V, Tian ZR, *Chem. Mat.* 2007, **19 (18),** 4454.

24. Anandan C, Dilli Babu P, Mohan L, *J. Mater. Eng. Perform,* 2013, **22(9),** 2623.

25. Taktaka S, Akbulut H, *Tribol. Inter.* 2007, **40**, 423.

26. Fernandes AC, Vaz F, Ariza E, Rocha LA, Ribeiro ARL, Vieira AC, Rivière JP, Pichon L, *Surf. Coat. Technol.* 2006, **200**, 6218.

27. Gokul Lakshmi S, Tamilselvi S, Rajendran N, Babi MAK, Arivuoli D, *Surf. Coat. Technol.* 2004, **182**, 287.

28. Gokul Lakshmi S, Raman V, Rajendran N, Babi MAK, Arivuoli D, *Sci. Technol. Adv. Mater.* 2003, **4**, 415.

29. Rolinski E. *Mater. Sci. Eng. A,* 1989, **108**, 37.

30. Mohan L, Anandan C, Grips VKW, *Appl. Surf. Sci.* 2012, **258**, 6331.

31. Mohan L, Dilli Babu P, Kumar P, Anandan C, *Surf. Interf. Anal.* 2013, **45**, 1785.

32. Prateek Kumar, Dilli Babu P, Mohan L, Anandan C, Grips VKW, *J. Mater. Eng. Perform.* 2013, **22,** 283.

33. Horcas I, Fernandez R, Gomez-Rodriguez JM, Colchero J, Gómez-Herrero JWSXM, Baro AM. *Rev. Sci. Instrum.* 2007, **78,** 013705.

34. Sulka GD, Parkoła KG, *Electrochim. Acta,* 2007, **52(5)**, 1880.

35. Liu YZ, Zu XT, Qiu SU, Cao J, Li CX, Huang XQ, Wei CF, *Vacuum,* 2006, **81**, 71.

36. Saha NC, Tompkins HG, *J. Appl. Phys.* 1992, **72**, 3072.

37. Milosev I, Kosec T, Strehblow HH, *Electrochim. Acta,* 2008, **53**, 3547.

38. Cheng Y, Zheng YF, *Surf. Coat. Technol.* 2007, **201**, 6869.

39. Mohan L, Anandan C, *Appl. Surf. Sci.* 2013, **268**, 288.

40. Kuznetsov MV, Ju.F. Zhuravlev, Zhilyaev VA, Gubanov VA, *J. Electron. Spectrosc. Relat. Phenom.* 1992, **58**, l.

41. Mohan L, Anandan C, *Appl. Surf. Sci.* 2013, **282**, 281.

42. Chusuei CC, Goodman DW, *Anal. Chem.* 1999, **71,** 149.

43. Anandan C, Mohan L. *J. Mater. Eng. Perform.* 2013, **22**, 3507.

44. Tamilselvi S, Raman V, Rajendran N, *Electrochim. Acta,* 2006, **52**, 839.

45. Mohan L, Anandan C, Grips VKW, *J. Mater. Sci. Mater. Med.* 2013, **24**, 623.

46. Mohan L, Anandan C, Rajendran N, *Mater. Sci. Eng. C,* 2015, **50**, 394.

47. Mohan L, Anandan C, Rajendran N, *Electrochimica. Acta,* 2015, **155**, 411.

Figure Captions

Fig. 1 FESEM images of TNT (a) and TNT+PN (b) (top view) inset water contact angle, (c and d) 3D images at higher magnification obtained from FESEM image and 2D profile of the nano tubes (e and f).

Fig. 2 FESEM images of (a) Ti-6Al-7Nb substrate and (b) Nitrided substrate.

Fig. 3 X-ray diffraction pattern for (a) Ti-6Al-7Nb substrate, (b) substrate nitrided at 800˚C, (c) TNT as-formed and (d) TNT + Nitrided at 800˚C.

Fig.4 Load versus displacement curve for (a) Substrate, (b) nitrided substrate, (c) TNT and (d) TNT + PN.

Fig. 5 FESEM images after NHT for TNT and TNT+PN samples (a and b), 3D images obtained from FESEM image (c and d) and (e and f) 2D profile of the nano indentation on TNT and TNT+PN.

Fig. 6 XPS core level spectra of Ti2p, N1s and O1s from (a) TNT and (b) TNT+PN samples.

Fig. 7 FESEM images of samples after 7days immersion in Hanks' solution **(a)** substrate, (**b)** TNT and **(c)** TNT + PN (inset at higher magnification).

Fig. 8 XPS survey spectra of (a) substrate, (b) TNT and (c) TNT+PN samples after 1 day immersion in Hanks' solution.

Fig. 9 XPS core level spectra of Ca2p, P2p and O1s from (a) substrate, (b) TNT and (c) TNT+PN samples after 1 day immersion in Hanks' solution.

Fig. 10 Potentiodynamic polarization curves for (a) substrate (b) nitrided substrate, (c) TNT and (d) TNT + PN samples.

Fig. 11 Nyquist plot (a), Bode plots (b) phase and (c) magnitude for substrate, nitrided substrate, TNT and TNT +PN samples.

Fig. 12 Equivalent circuit (EC) diagram used for fitting EIS data of the substrate and nitrided substrate (a) and (b) TNT and TNT+PN samples.

Table 1: Composition of TNT and TNT + PN samples obtained by XPS.

Sample	Ti2p at.%	O1s at.%	N1s at.%	N	
				TiN %	TiNxOy %
TNT	17.9	82.1	-	-	-
TNT+PN	20.7	72.0	7.3	65.4	34.6

Table 2: Composition of Ti2p, Ca2p, P2p and O1s after 1day immersion in Hanks' solution obtained by XPS.

Sample	Ti2p at.%	Ca2p at.%	P2p at.%	O1s at.%
Substrate	5.9	14.6	12.9	66.6
TNT	1.9	21.0	18.8	58.3
TNT+PN	3.7	17.0	14.5	64.8

Table 3: Results of potentiodynamic polarization studies.

S. no	Sample	E_{corr} (V)	i_{corr} ($\mu A/cm^2$)
1.	Substrate	-0.303	0.0058
2.	Nitrided substrate	-0.188	0.0266
3.	TNT	-0.236	0.0158
4.	TNT + PN	-0.308	0.0990

Table 4: Electrochemical impedance parameters obtained by fitting equivalent circuit model for substrate, nitrided substrate, TNT and TNT + PN samples

Samples	R_e	Q_1	n_1	R_1	Q_2	n_2	R_2	Q_3	n_3	R_3	χ^2
	Ω cm^2	S s^n cm^{-2}		Ω cm^2	S s^n cm^{-2}		Ω cm^2	S s^n cm^{-2}		Ω cm^2	
Substrate	14	7.3×10^{-8}	0.98	21.5	1.7×10^{-5}	0.92	5.8×10^{6}	-	-	-	5.5×10^{-4}
Nitrided substrate	15	6.8×10^{-8}	0.96	21.5	3.1×10^{-5}	0.88	5.4×10^{6}	-	-	-	5.3×10^{-4}
TNT	11	1.3×10^{-7}	0.91	27.5	1.6×10^{-5}	0.92	1.5×10^{4}	5.4×10^{-6}	0.92	5.6×10^{6}	2.5×10^{-4}
TNT+PN	16	8.5×10^{-8}	0.96	34.5	5.4×10^{-4}	0.79	58	6.2×10^{-5}	0.90	5.2×10^{6}	4.2×10^{-4}

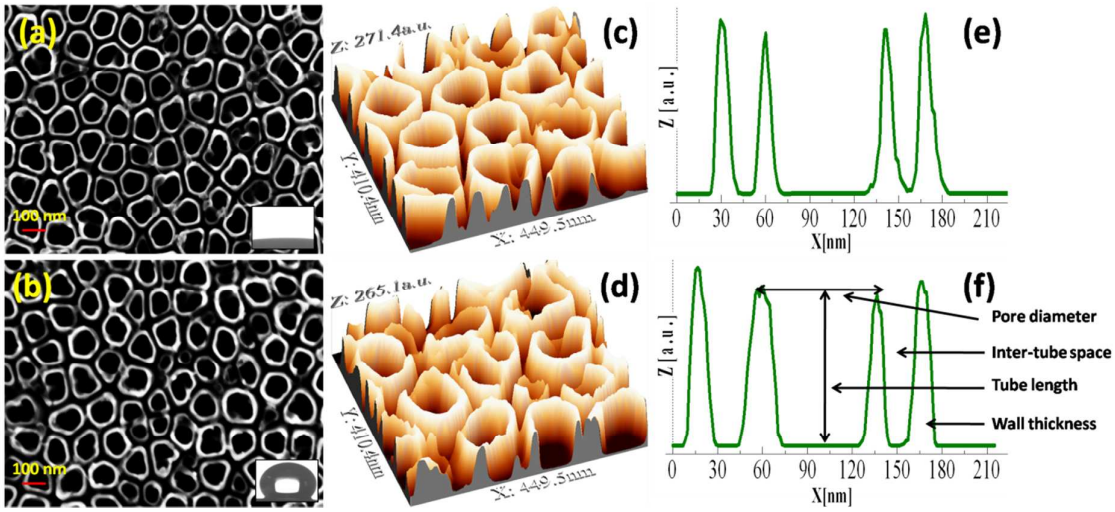

Fig. 1 FESEM images of TNT (a) and TNT+PN (b) (top view) inset water contact angle, (c and d) 3D images at higher magnification obtained from FESEM image and 2D profile of the nano tubes (e and f).

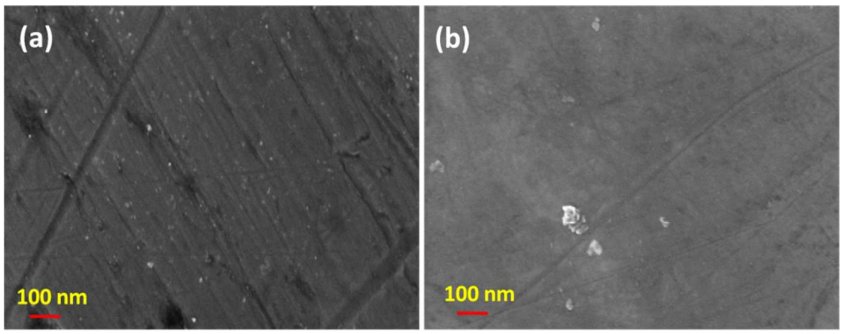

Fig. 2 FESEM images of (a) Ti-6Al-7Nb substrate and (b) Nitrided substrate.

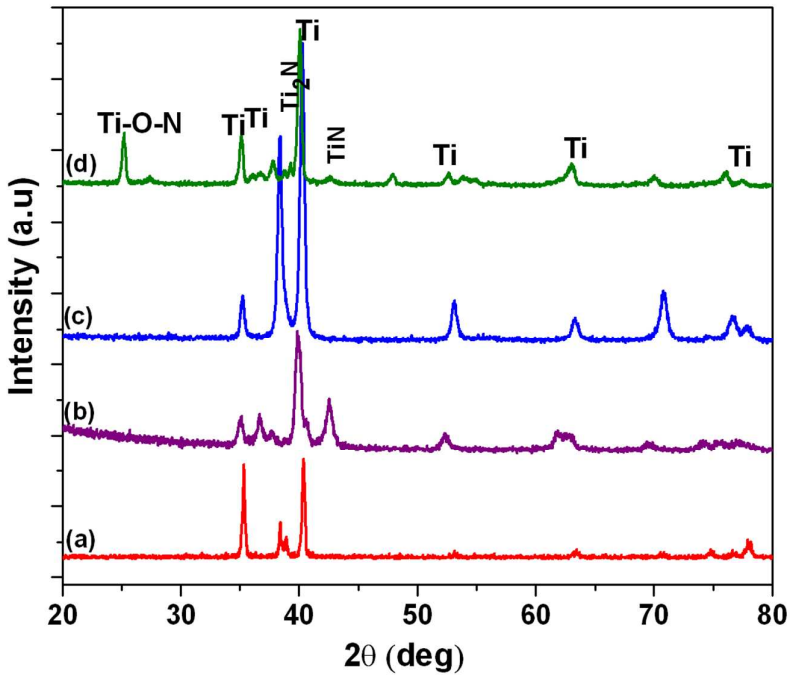

Fig.3 X-ray diffraction pattern for (a) Ti-6Al-7Nb substrate, (b) substrate nitrided at 800˚C, (c) TNT as-formed and (d) TNT + Nitrided at 800˚C.

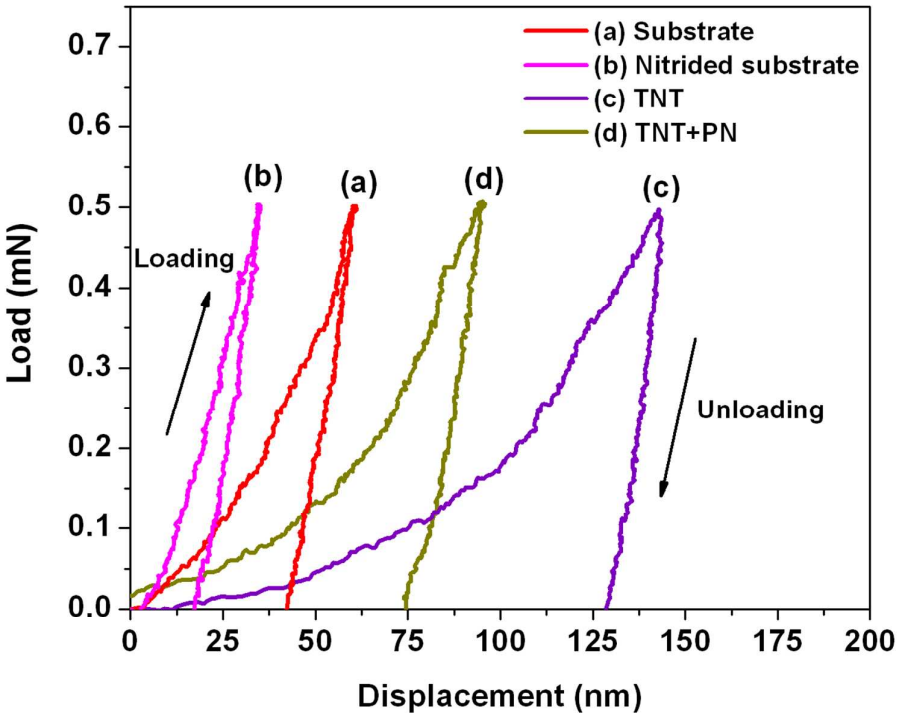

Fig.4 Load versus displacement curve for (a) Substrate, (b) nitrided substrate, (c) TNT and (d) TNT + PN

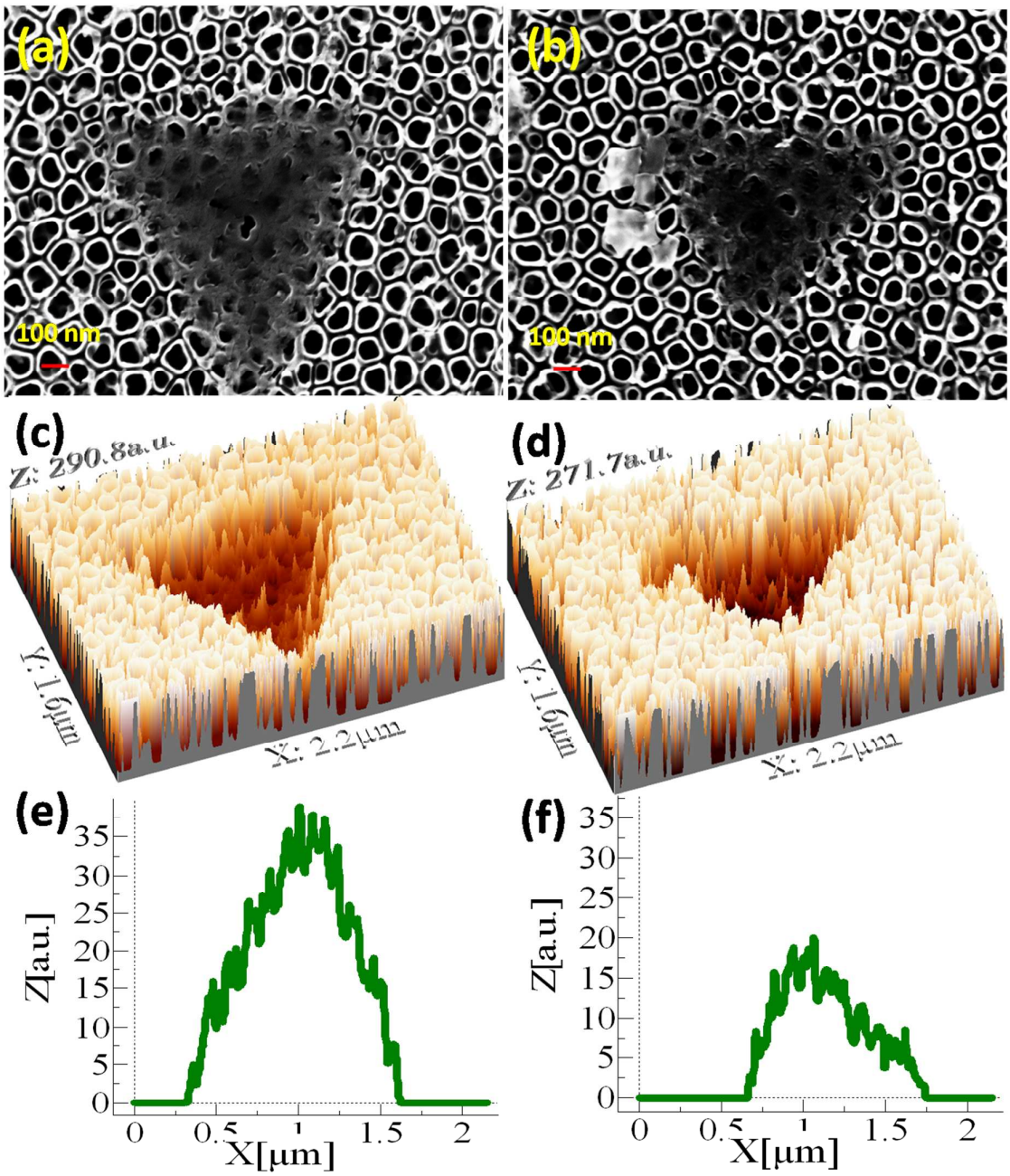

Fig. 5 FESEM images after NHT for TNT and TNT+PN samples (a and b), 3D images obtained from FESEM image (c and d) and (e and f) 2D profile of the nano indentation on TNT and TNT+PN.

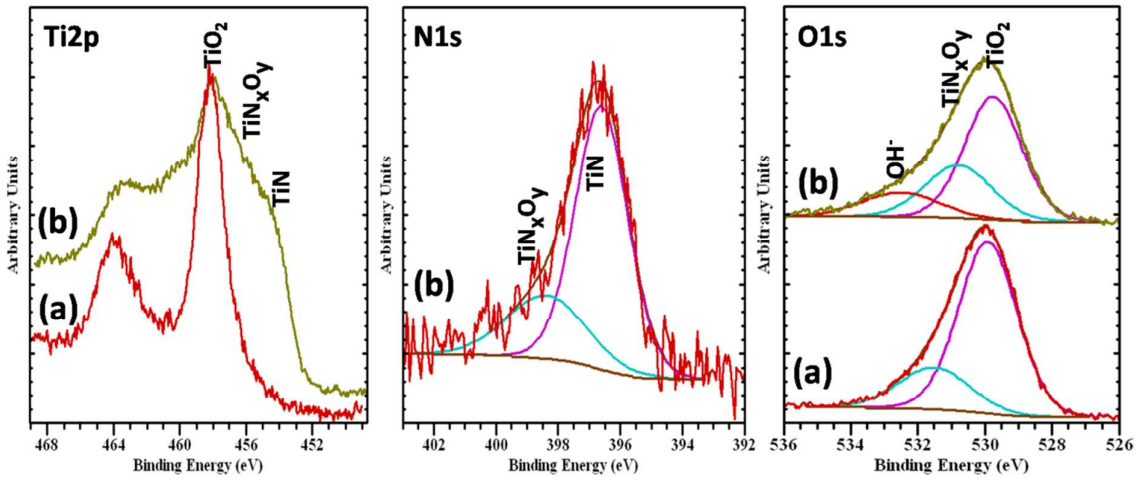

Fig. 6 XPS core level spectra of Ti2p, N1s and O1s from (a) TNT and (b) TNT+PN samples.

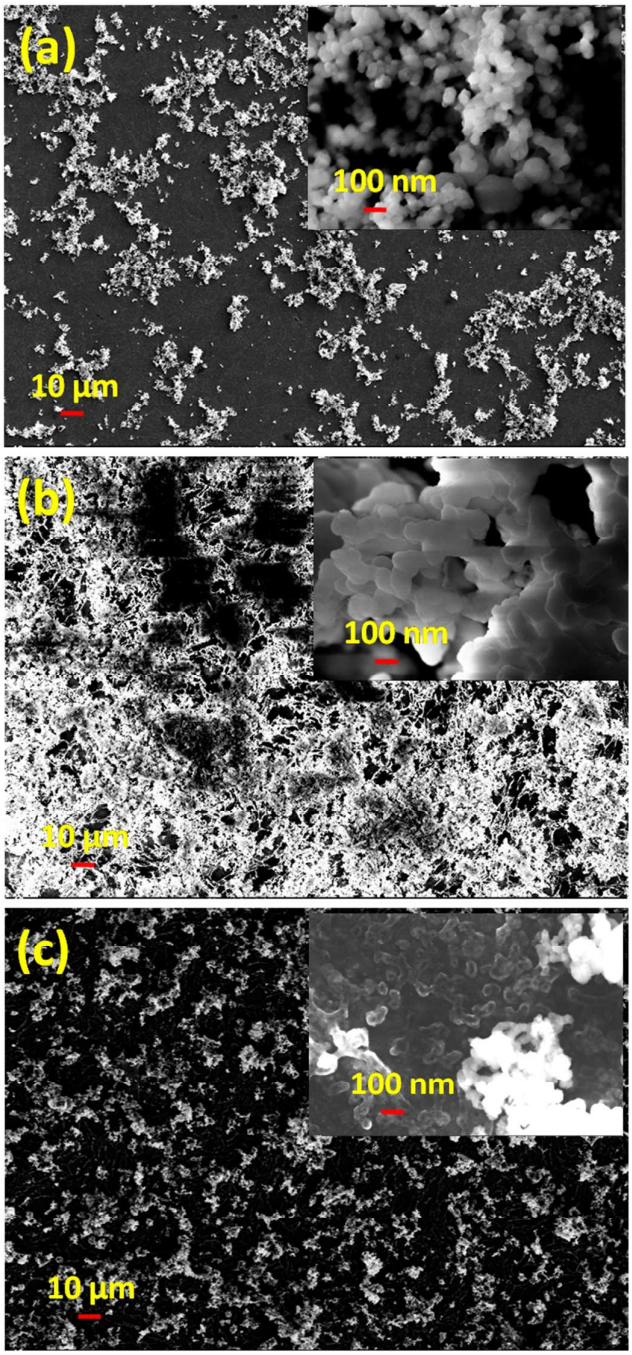

Fig. 7 FESEM images of samples after 7days immersion in Hanks' solution **(a)** substrate, (**b)** TNT and **(c)** TNT + PN (inset at higher magnification).

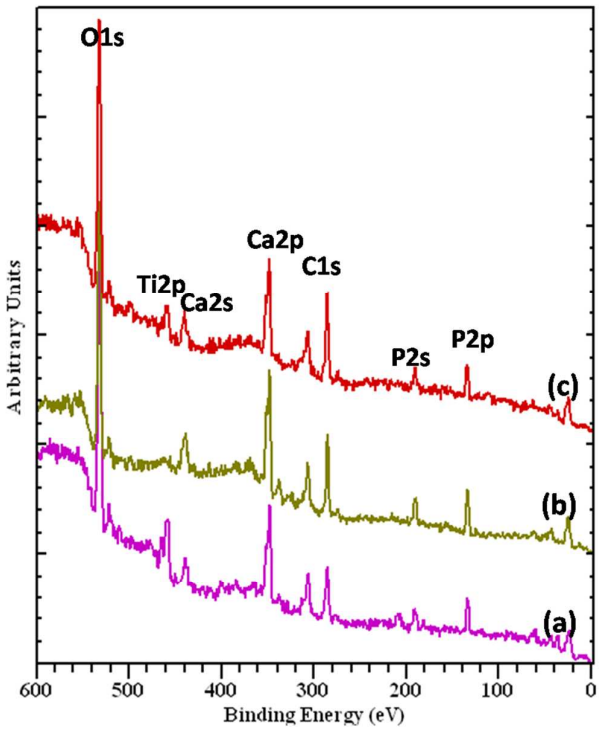

Fig. 8 XPS survey spectra of (a) substrate, (b) TNT and (c) TNT+PN samples after 1 day immersion in Hanks' solution.

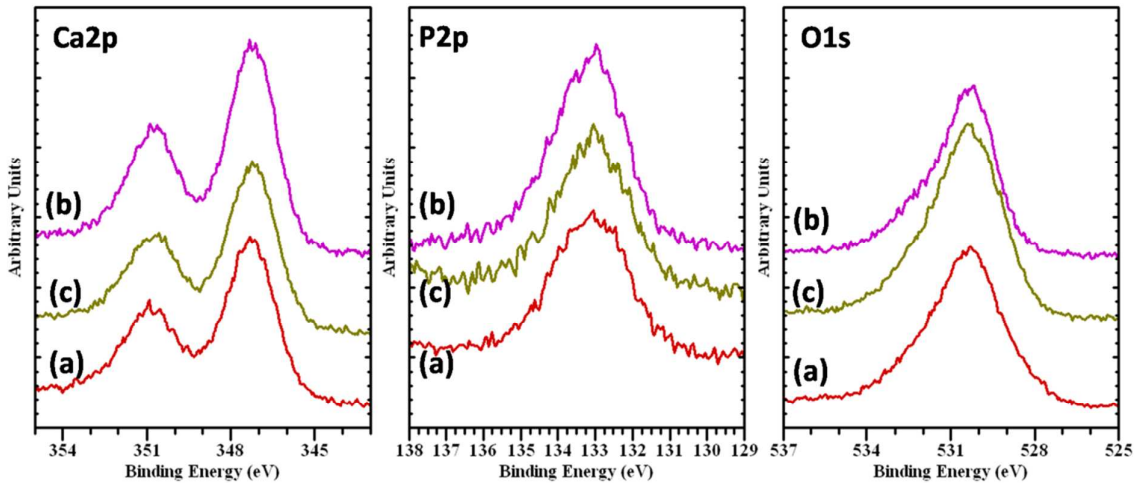

Fig. 9 XPS core level spectra of Ca2p, P2p and O1s from (a) substrate, (b) TNT and (c) TNT+PN samples after 1 day immersion in Hanks' solution.

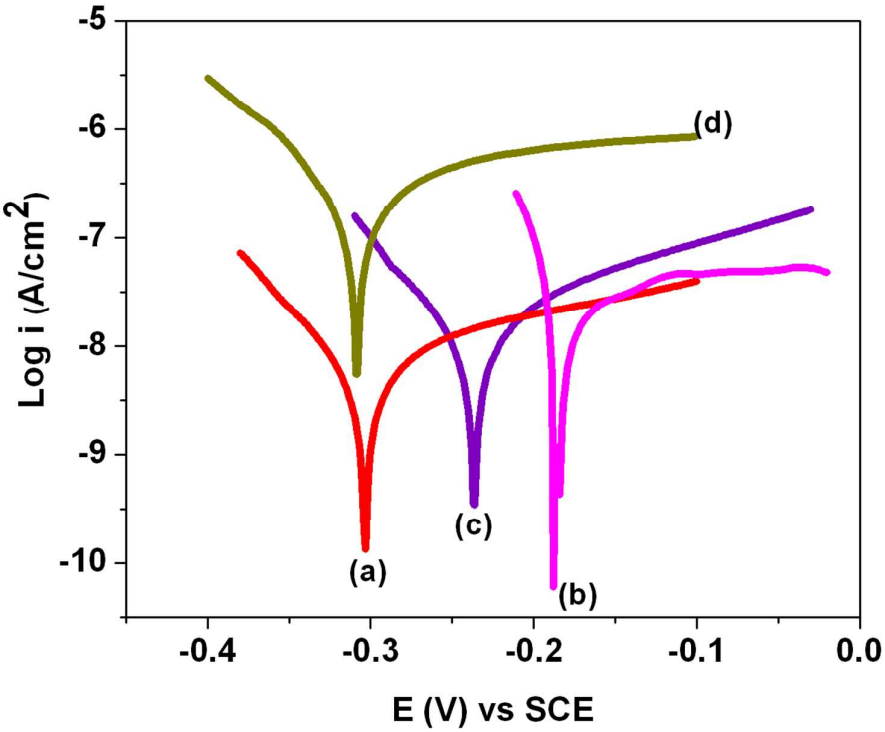

Fig. 10 Potentiodynamic polarization curves for (a) substrate (b) nitrided substrate, (c) TNT and (d) TNT + PN samples.

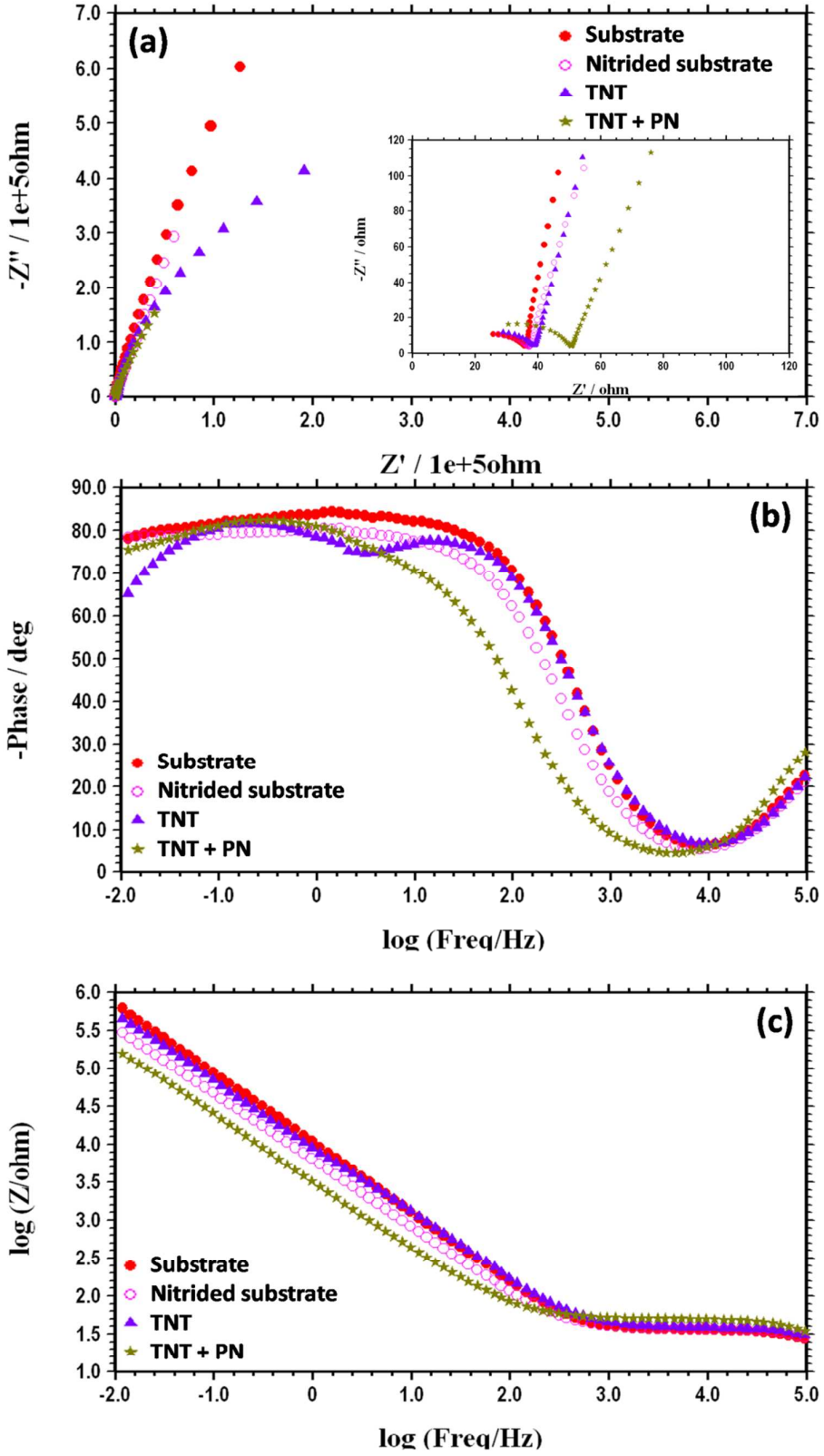

Fig. 11 Nyquist plot (a), Bode plots (b) phase and (c) magnitude for substrate, nitrided substrate, TNT and TNT +PN samples

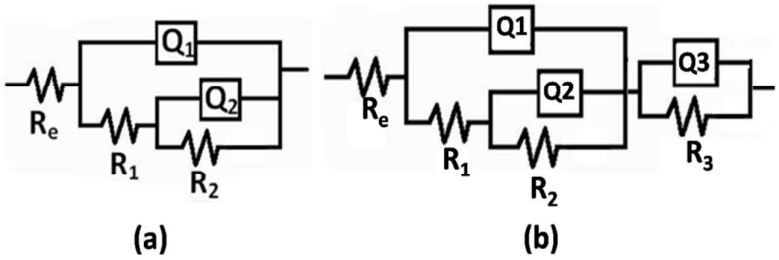

Fig. 12 Equivalent circuit (EC) diagram used for fitting EIS data of the substrate and nitrided substrate (a) and (b) TNT and TNT+PN samples.